Hydrol. Earth Syst. Sci., 17, 4851–4863, 2013
www.hydrol-earth-syst-sci.net/17/4851/2013/
doi:10.5194/hess-17-4851-2013

Hydrology and Earth System Sciences
Open Access

Indirect downscaling of hourly precipitation based on atmospheric circulation and temperature

F. Beck and A. Bárdossy

University of Stuttgart, Institute for Modelling Hydraulic and Environmental Systems, Stuttgart, Germany

Correspondence to: F. Beck (ferdinand.beck@iws.uni-stuttgart.de)

Received: 19 June 2013 – Published in Hydrol. Earth Syst. Sci. Discuss.: 8 July 2013
Revised: 14 October 2013 – Accepted: 30 October 2013 – Published: 5 December 2013

Abstract. The main source of information on future climate conditions are global circulation models (GCMs). While the various GCMs agree on an increase of surface temperature, the predictions for precipitation exhibit high spread among the models, especially in shorter-than-daily temporal resolution. This paper presents a method to predict regional distributions of the hourly rainfall depth based on daily mean sea level pressure and temperature data. It is an indirect downscaling method avoiding uncertain precipitation data from the GCM. It is based on a fuzzy logic classification of atmospheric circulation patterns (CPs) that is further subdivided by means of the average daily temperature. The observed empirical distributions at 30 rain gauges to each CP-temperature class are assumed as constant and used for projections of the hourly precipitation sums in the future. The method was applied to the CP-temperature sequence derived from the 20th-century run and the scenario A1B run of ECHAM5. For the study region in southwestern Germany ECHAM5 predicts that the summers will become progressively drier. Nevertheless, the frequency of the highest hourly precipitation sums will increase. According to the predictions, estival water stress and the risk of extreme hourly precipitation will both increase simultaneously during the next decades. However, the results are yet to be confirmed by further investigation based on other GCMs.

1 Introduction

The main source of information on future climate conditions are global circulation models (GCMs). While the various GCMs agree on an increase of surface temperature, the predictions for precipitation exhibit high spread among the models. The complex physics of precipitation genesis results in high spatial and temporal heterogeneity, which cannot be represented to the full extent by the GCMs.

On the global scale an increase in precipitation is expected during the 21st century due to enhanced evaporation under warmer climatic conditions. The GCMs used in the IPCC's fourth assessment report predict a global precipitation increase of 1 to 3 % per °C of global warming (Held and Soden, 2006). Wentz et al. (2007) estimated the relation between average global temperature and total global precipitation volume from satellite observations and found a rate of 7.4 % (with a possible error of ±2.6 %) per degree Celsius. The rate is in agreement with the Clausius–Clapeyron relation, which states that the moisture capacity of the air increases by about 7 % per 1°C. Over the oceans evaporation is mainly governed by the moisture capacity. A warmer atmosphere can evaporate and carry more water, which has to fall down somewhere so that the mass balance is fulfilled.

Regional changes in precipitation, however, differ from the Clausius–Clapeyron increase rate since they are governed not only by potential evaporation and atmospheric moisture capacity, but also by changes in other factors, e.g. atmospheric circulation or soil moisture. In an extensive study comparing several runs of AM3P from the Met Office Hadley Centre, UK, Kendon et al. (2010) evaluated the effects of global changes in different climatic factors on regional precipitation. According to the model, one of the key factors for most parts of Europe is soil moisture depletion, leading to drier conditions during summer months when atmospheric temperature is rising (Kendon et al., 2010).

In observed time series regional deviations from the Clausius–Clapeyron relation have been found, too. In central Europe during the second half of the 20th century

temperature had been increasing, but an increase in precipitation volume could not be observed. An increase during winter months was balanced by a decrease during summer (Hundecha and Bárdossy, 2005). Simultaneously, daily precipitation extremes had become more pronounced (Hundecha and Bárdossy, 2005), indicating a shift in the distribution. Both trends are confirmed by climate model runs and are predicted to continue in the future, e.g. by the PRUDENCE ensemble study of 19 combinations of global and regional circulation models (RCMs) (see Déqué et al. (2007) for the seasonal shift, Fowler et al. (2007) for the extremes).

Most studies analyzing GCM output deal with monthly or daily precipitation sums. Although GCMs exhibit a temporal resolution of up to 30 min, sub-daily values are generally discarded. Due to the limited spatial resolution of GCMs, convective events, which are responsible for the highest precipitation intensities, can only be modeled conceptually (Trenberth et al., 2003). The parameterization of convection, however, is still problematic (Guichard et al., 2004). Hence, it is assumed that model errors are highest in the shortest time steps, where convection plays a major role. To avoid the application of uncertain GCM data, climate predictions of sub-daily precipitation amounts are generally based on spatial-temporal downscaling of daily values.

Downscaling can be done dynamically by nesting an RCM with higher resolution but limited spatial extent in the global model and/or by statistical methods. While dynamical downscaling is based on physical information finding its expression in the equations of the RCM, statistical downscaling is merely based on the statistical relation of precipitation on different scales, e.g. of daily and sub-daily resolution. In general, statistical downscaling methods are calibrated with data from past time observations. The established relation is then applied to the GCM data of the future. Nguyen et al. (2007) developed a downscaling scheme that links daily and hourly precipitation extremes by a multiple linear regression approach that takes spatial correlations into account. Another possibility are cascade models that link precipitation of different spatial-temporal resolution by the multi-fractal scaling characteristics (e.g. Molnar and Burlando, 2005). As they exhibit a low number of parameters and an easy model fit, they are frequently used for downscaling applications. Groppelli et al. (2011) for example use a random cascade model to provide precipitation data for catchment models by spatial downscaling of daily GCM precipitation sums. The grid cells of the GCM are about 200 km^2; the target scale of the catchment model is 2×2 km. Willems and Vrac (2011) compare several other downscaling methods, e.g. the delta change method and the analogues method. In the delta change method, the absolute precipitation values of the GCM are discarded; only the trend signal (the delta change) is kept, which is used to modify locally observed distributions of the past. Lenderink et al. (2007) examine the effect of the delta change method on river discharges simulated in a hydrological model. While the average discharges are similar to the discharges calculated directly from RCM precipitation, the extremes are much higher when delta-changed data are applied. The analogues method does not use any precipitation data from the GCM, but it uses observed precipitation from past days as predictions for the future. The choice of the past days that are assigned to the GCM output is based on a similarity measure, e.g. of the predicted atmospheric circulation.

The application of statistical downscaling in climate change studies implies the assumption that the relation between the scale of the GCM and the target scale is constant over time. Concerning precipitation, the assumption becomes problematic if the temporal target resolution is shorter than one day, since there is strong evidence that global warming affects the relation between daily and sub-daily precipitation sums. An examination based on data from several hundred rain gauges in southwestern Germany revealed changes in the temporal scaling. The portion of the daily sum that can fall within one hour has been increasing during the second half of the 20th century. This increase concerns the extremes as well as average events (Beck, 2013, p.153–157).

For De Bild, Netherlands, it was found that the 99 % quantile of hourly precipitation amounts increases by twice the Clausius–Clapeyron relation if the atmospheric temperature exceeds 14°C, while the 99 % quantile of daily sums grows by the Clausius–Clapeyron rate of 7 % per °C (Lenderink and van Meijgaard, 2008). It proves that the relation between hourly and daily precipitation is temperature-sensitive and, therefore, will react to global warming. A subsequent study revealed similar behavior in Hong Kong, under subtropical climatic conditions (Lenderink et al., 2011). Thus, the findings are not limited to temperate climate, but might probably indicate a universal property of precipitation. Trenberth et al. (2003) predicted such a behavior, called "super Clausius–Clapeyron", for convective precipitation events assuming a positive feedback effect at the onset of condensation: the higher absolute moisture content of a warmer atmosphere leads to a stronger latent heat release during condensation, which in turn reinforces the convective uplift responsible for condensation (Trenberth et al., 2003).

If a constant relation is assumed between daily and hourly precipitation, super Clausius–Clapeyron behavior is ignored, resulting in a problematic underestimation of extreme hourly precipitation frequencies. Therefore, any temporal downscaling method used in climate change studies requires additional information to represent changes in the relation of daily to sub-daily precipitation. The presented dowscaling scheme uses atmospheric circulation patterns (CPs) and temperature as additional information. The CPs are seen as the link between the large-scale atmospheric flow field and the local precipitation response, temperature as a climatic key factor triggering local changes in convective uplift and moisture capacity.

The downscaling scheme is an indirect method, avoiding any GCM precipitation data. Instead, it relies on predictions of MSLP and atmospheric temperature, which are considered

as more reliable (see for example Kendon and Clark, 2008). The output of this method is expected future distributions of hourly precipitation which, in a next step, can be used as basis for stochastic time series simulation.

In this case study, we provide predictions of hourly precipitation for the federal state of Baden-Württemberg in the southwest of Germany (about 35 000 square kilometers). The predictions are based on data from two ECHAM5 runs. In subsequent studies, the presented downscaling scheme should be applied to scenario runs of many different GCMs to improve the robustness of the results.

In the next section the methodology of the CP classification system is explained and how it is used for downscaling purposes.

In Sect. 3 the observed CP sequence between 1958 and 2003 is analyzed. CPs which frequently lead to high hourly precipitation sums are identified and trends in the CP sequence estimated. It is investigated how the CPs react to temperature.

Section 4 gives a prognosis on the CP sequence until 2060 based on the global circulation model ECHAM5. Expectations for the yearly precipitation sum and the probability for extreme hourly precipitation sums are derived from the CP sequence.

The paper concludes with an estimation of the reliability of the projected trends in hourly precipitation.

2 Methodology

2.1 Fuzzy-rule-based CP classification

The proposed downscaling method is based on a circulation pattern (CP) classification of the atmospheric flow field. The CPs result from an objective and automated classification. It follows the method described by Bárdossy (2010), except for modifications concerning the objective function. The CPs are further subdivided into temperature classes to take the temperature sensitivity of the relation between large-scale circulation and local precipitation response into account.

2.2 Choice of the CP class

The classification is performed by a fuzzy rule set based on normalized MSLP anomalies. The pressure data are derived from the NCEP/NCAR reanalysis (Kistler et al., 2001) with a temporal resolution of one day and a spatial resolution of 2.5° by 2.5°.

Based on the pressure anomalies, five fuzzy states are defined:

1. large positive anomalies,
2. medium positive anomalies,
3. medium negative anomalies,
4. large negative anomalies,
5. arbitrary.

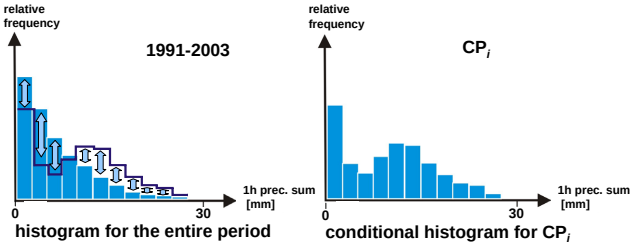

Fig. 1. Principle of the objective function for the CP definition in the simulated annealing scheme.

The rule set defining the n_{cp} CPs specifies the required fuzzy state for each of the grid points. It can be described by a matrix:

$$\mathbf{V} = v(i,j);\ i = 1,\ldots n_{\mathrm{pts}};\ j = 1,\ldots n_{\mathrm{cp}}. \quad (1)$$

The definition of one CP class j consists of the state index $v = [1,5]$ to each grid point i of the n_{pts} grid points in the MSLP-anomalies field over Europe and the North Atlantic Ocean. The state "arbitrary" is assigned to all points that are indifferent to the respective weather type definition. For each day the current anomaly field is compared with the CP-defining fuzzy rule set. The CP with the highest resemblance, resulting in the highest degree of fulfillment (DOF) of the fuzzy rule, is chosen as the CP of the day. All days that cannot be assigned to any of the the n_{cp} predefined CPs, because the DOF is below a certain threshold, are assigned to the additional class "CP99".

2.3 Definition of the rule set

The rule set which forms the classification system is not predefined, but found by a stochastic optimization. The objective function O of this optimization is adapted to the specific problem: e.g. for the identification of flood-producing CPs, the increase rate of river discharges can be used as the objective function (Bárdossy and Filiz, 2005) or the spatial coverage of stations with significant rainfall (Bárdossy, 2010). In this study the classification is used as a link between large-scale atmospheric circulation and regional hourly rainfall depths. Therefore, the objective function O is designed to quantify the differences in the distribution of 1 h precipitation amounts that are induced by the CP classification. The first part of O, according to the sketch in Fig. 1, is equivalent to the statistical variable χ^2, which is the sum of the squared residuals in relative frequency $h_i(j)$ between the histogram class j for all days belonging to one CP i and the same histogram class for the climatic average $h_{\mathrm{clim}}(j)$

without classification:

$$\chi^2 = \sum_{i=1}^{n_{cp}} \sum_{j=1}^{k} (h_i(j) - h_{clim}(j))^2 \rightarrow \max! \quad (2)$$

(χ^2 is equal to the sum of the squared lengths of the arrows in Fig. 1.) As a second part of O, the difference of the CPs to the climatic average in hourly rainfall frequency $P_{1\,\mathrm{h}}(R \geq 0.1\,\mathrm{mm})$ is included to distinguish between wet and dry CPs.

The optimization is performed by a simulated annealing algorithm (Aarts and van Laarhoven, 1989) which starts with an initial random fuzzy rule set and, thus, a meaningless CP classification. In the beginning the distribution of all CPs will be very similar: χ^2 close to zero. Then the optimization arbitrarily chooses grid points, alters the fuzzy anomaly state at these points and evaluates the performance of the resulting classification system by the value of the objective function O. Changes that improve O are kept; changes that worsen O are kept by a certain probability, which is decreasing during the course of the optimization. In the course of the optimization the classification becomes more and more meaningful, and so the distributions more and more different. The optimal classification is found if the CPs differ as much as possible in their statistical properties, and the objective function O is at its max.

The number of CPs n_{cp} is not part of the optimization the but choice of the modeler. In this respect, the classification is subjective. By different precipitation-related performance measures, Bárdossy (2010) estimated an optimal number of CPs varying between 16 and 20, depending on the applied objective function. In this study, however, in perspective of the following temperature subdivision, the number of CPs is reduced to $n_{\mathrm{cp}} = 12$ in favor of stable estimates of the histogram class frequencies. (With an even lower number of CPs, the frequency of days that cannot be assigned to any CP class increases significantly, an indication that a considerably part of the information gets lost.)

The frequencies $h_i(j)$ and $P_{1\,\mathrm{h}}$ are calculated based on the hourly records of 30 rain gauges spread all over the study area of Baden-Württemberg (see Fig. 2). To make the rainfall depths of all 30 stations comparable, histogram classes are defined at each station individually according to the local CDF. Then the relative frequency of each class j of each CP i is averaged over all stations. To avoid implicit weighting due to unequal data availability, the method requires close to complete hourly rain depth records. For this reason, the calibration period, for which the histograms are calculated, is limited to the time span from 1991 to 2003.

The limits of the $j \in [1, k]$ histogram classes are defined by the empirical quantiles to predefined CDF values. To shift the focus towards high precipitation amounts, the classes are not equidistant in CDF but smaller for higher CDFs. The upper limits of the histogram classes are $F^{-1}(0.6)$, $F^{-1}(0.8)$, $F^{-1}(0.9)$, $F^{-1}(0.95)$, $F^{-1}(0.98)$, $F^{-1}(0.99)$ and $F^{-1}(1.0)$, which means that the last class is open to the right. The CDFs are calculated from all wet hours with no less than 0.1 mm of precipitation.

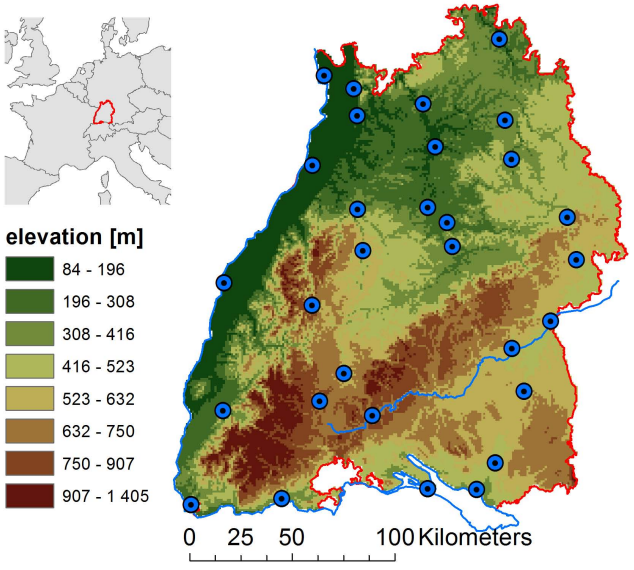

Fig. 2. Set of 30 high resolution rain gauges with continuous measurements from 1991 to 2003 and low number of missing values.

While the CP-defining fuzzy rule set is constant over the year, the histograms are calculated for two seasons, from September to April and from May to August to account for seasonal effects in the precipitation response of the CPs, especially convective precipitation enhancement during summer months.

2.4 Temperature subdivision

The 12 CP classes are further subdivided according to the average observed daily air temperature at 156 measurement stations in Baden-Württemberg, which is seen as an approximation of atmospheric temperature governing potential evaporation and the occurrence of convection. The subdivision is made by the observed temperature CDF to each CP. The 20 % of days with the coldest average temperature in each CP class are declared "*cold*", the next 20 % "*cool*", followed by "*avg*", "*warm*" and "*hot*" conditions. To avoid seasonal effects, the quantiles are calculated on the basis of anomalies from the average yearly cycle. The assigned temperature class is relative to the CP. The same temperature anomaly can be declared as *cool* or *warm*, depending on whether the corresponding CP leads to southern, generally warmer, or northern, generally cooler, fluxes.

2.5 CP-temperature classification as downscaling tool

The CP-temperature classification has three results: first the CP-defining fuzzy rule set, second the daily sequence of CP-temperature classes from 1991 to 2003, and third the

Table 1. Main SLP characteristics of the twelve CPs, average rain day frequency P_{1d} and average wet day rainfall depth $\bar{R}_{1d}$ with a threshold of $R \geq 0.1$ mm.

Name	Main SLP features	P_{1d} $\bar{R}_{1d}$
CP1	positive anomalies over Scotland	51.8 %
	negative anomalies over Sicily	3.85 mm
CP2	positive anomalies from England to Austria	52.6 %
	negative anomalies over Island	3.86 mm
CP3	positive anomalies over eastern Germany	44.4 %
	negative anomalies over Island	1.36 mm
CP4	positive anomalies west of Ireland	64.4 %
	negative anomalies over Estonia	3.25 mm
CP5	positive anomalies over Scotland	43.1 %
		2.02 mm
CP6	positive anomalies over England	56.9 %
		3.66 mm
CP7	positive anomalies over Spain	85.9 %
	negative anomalies over southern Norway	5.52 mm
CP8	positive anomalies over France	57.7 %
	negative anomalies south of Island	2.67 mm
CP9	positive anomalies east of Island	47.8 %
	negative anomalies over the Iberian Sea	2.44 mm
CP10	positive anomalies over Island	80.7 %
	negative anomalies between England and Denmark	5.21 mm
CP11	positive anomalies west of Ireland	86.3 %
	negative anomalies over Poland	7.27 mm
CP12	negative anomalies between Scotland and Norway	77.8 %
		5.94 mm

empirical distribution of hourly precipitation sums of each CP-temperature combination in each of the two seasons (September to April and May to August) at the 30 precipitation stations. The spatial-temporal downscaling effect of the classification is in the latter: information on hourly precipitation values on a regional scale is associated with daily information of large-scale atmospheric circulation and temperature.

The CP-defining fuzzy rule set can be applied to gridded daily MSLP data of any GCM. The only condition is that the spatial resolution is comparable to the resolution of the NCEP/NCAR reanalysis. In this study it is applied to data from two runs of ECHAM5 from the Max Planck Institute in Hamburg, Germany (Roeckner et al., 2003). The temperature subdivision is based on the average daily temperature of the four ECHAM5 grid points over the study region (latitudes of 47.564° N and 49.429° N and longitudes of 7.5° E and 9.375° E.)

Thus, pressure and temperature data are transformed into a time series of daily CP-temperature classes. If it is assumed that the distribution of hourly precipitation sums to each CP-temperature class in each season (September to April and May to August) does not change over time, the observed

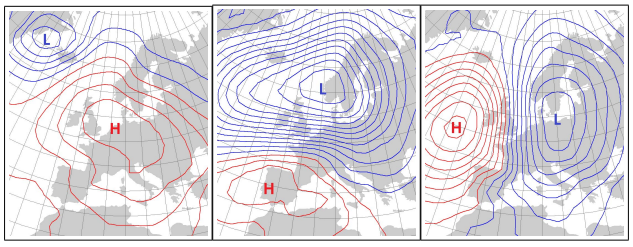

(a) CP2 (b) CP7 (c) CP11

Fig. 3. 1 hPa isobars of the mean sea level pressure anomalies of CPs related to high precipitation intensities.

statistics during the calibration period from 1991 to 2003 can be used to derive prognosis of the hourly precipitation statistics from the CP-temperature sequence of the GCM run. The average observed cumulated histogram frequencies are seen as a prediction of the CDF, and the observed rainfall frequency as the expected rainfall probability. Taking the CP-temperature sequence of one target year from the GCM run, the predicted yearly distribution is calculated as the weighted average of the distribution to each CP-temperature class. The weights are the relative frequencies of the CP-temperature classes in each of the two seasons. In a next step, other statistics can be derived from the expected distributions of the target year, e. g. the exceedance frequency of each histogram limit or the expected yearly precipitation sum.

3 CP classification according to NCEP/NCAR reanalysis data

Table 1 gives an overview of the main features, the rain day frequency and the average wet day rainfall depth of the twelve CPs derived from the NCEP/NCAR reanalysis data set during the calibration period from 1991 to 2003. The threshold for a "wet" day is a rainfall depth of no less than 0.1 mm. CPs with anticyclonic conditions in the study region (CP2, CP3, CP5 and CP8) lead to relatively dry conditions. CPs during which the study region is in the zone of influence of cyclonic depressions (CP7, CP9, CP10 and CP11) lead to the highest average wet day sums.

3.1 CPs with potential for high hourly precipitation sums

In perspective of the downscaling scheme, the differences in hourly precipitation are the most crucial. The maps in Fig. 3 show the average pressure anomalies according to the NCEP/NCAR data set of all days belonging to three CPs which frequently lead to high hourly precipitation sums. CP2 is a high-pressure situation with generally weak atmospheric exchange. CP7, with the low-pressure center over the south of Norway, generates western to northwestern fluxes. CP11 generates northern fluxes between the high-pressure zone over the Atlantic ocean and the low-pressure zone over

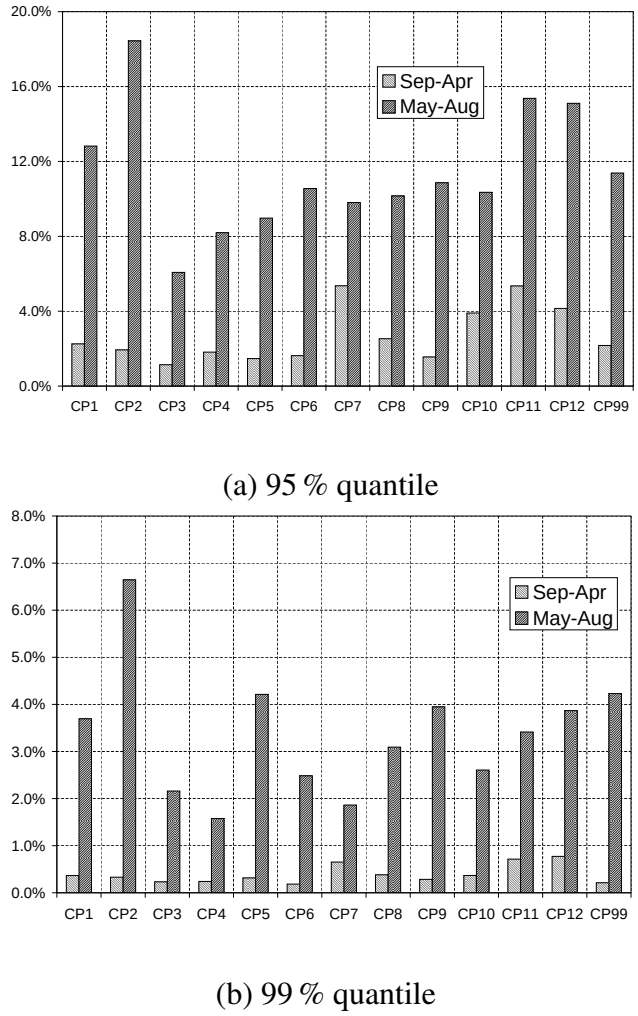

Fig. 4. Exceedance frequency of the 95 % and 99 % quantile for two seasons; quantiles and frequencies are calculated for all hours with $R \geq 0.1$ mm.

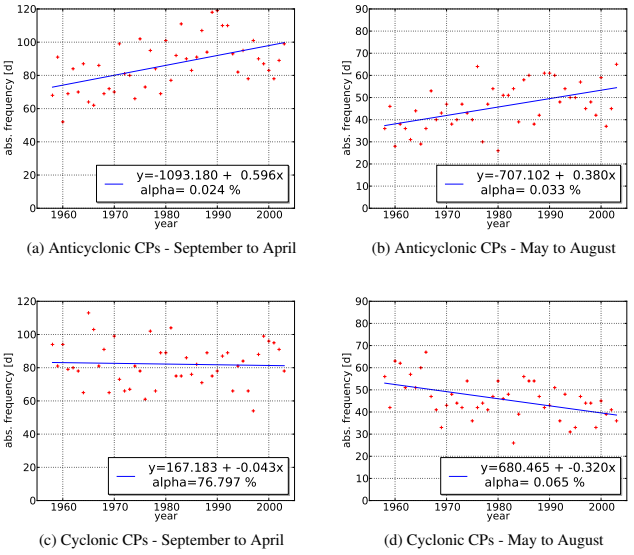

Fig. 5. Trends in the frequency of anticyclonic (CP2, CP3, CP5 and CP8 – first line) and cyclonic CPs (CP7, CP10, CP11 and CP12 – second line) according to NCEP/NCAR reanalysis.

eastern Europe. It might seem surprising at first that CP2 is among the CPs with highest potential for intensive precipitation (Fig. 3a) since high-pressure situations generally lead to dry conditions and, thus, the rain day frequency and average daily sums of CP2 are rather low. If it rains, however, convective events can provoke high intensities, especially during summer months.

Figure 4 displays the relative exceedance frequencies of the 95 % and 99 % quantile of all wet hour precipitation amounts during the calibration period from 1991 to 2003. On average over all CPs and both seasons the frequency is 5 %, respectively 1 %. High intensities are generally more frequent during summer months. The highest intensities are mainly produced by convective precipitation events. In winter convective events are bound to turbulent mixing at cold fronts. During summer months the increased solar heating is an additional driving force for convection and even triggers events that are not bound to an approaching front. Therefore, the estival increase in the 95 % and 99 % quantile exceedance frequencies indicates the influence of convection. The anticyclonic CP2 exhibits an elevated potential for high hourly sums only during summer months, while the frequency of CP11 with turbulent northern fluxes is among the highest during both seasons. CPs with westerly fluxes as CP7 are less influenced by convective intensity enhancement and show the lowest increase in the 95 % and 99 % quantile exceedance frequencies during summer months.

3.2 Changes in the CP Sequence

For an analysis of potential trends in atmospheric circulation, the fuzzy rule set derived from the 1991 to 2003 calibration period was applied to a longer time series of NCEP/NCAR MLSP fields from 1958 to 2004. To reduce spread due to random variations, the CPs were grouped according to their meteorological characteristics. Fig. 5 displays the absolute yearly occurrence frequencies of anticyclonic CPs (CP2, CP3, CP5 and CP8 – first line) and cyclonic CPs (CP7, CP10, CP11 and CP12 – second line) between 1958 and 2004. During the CP calibration period from 1991 to 2003, one of the anticyclonic CPs occurred on 35.6 % of all days, but only 17.5 % of all rainy hours at the 30 rain gauges used for calibration were counted during that time. One of the cyclonic CPs occurred on 30.0 % of all days. They are responsible for 55.4 % of all hours with non-zero precipitation.

Potential trends in the CP sequence between 1958 and 2004 (NCEP/NCAR) are quantified by linear regression and marked by a line in Fig. 5. The significance of the regression is evaluated by a two-sided hypothesis test. The value of

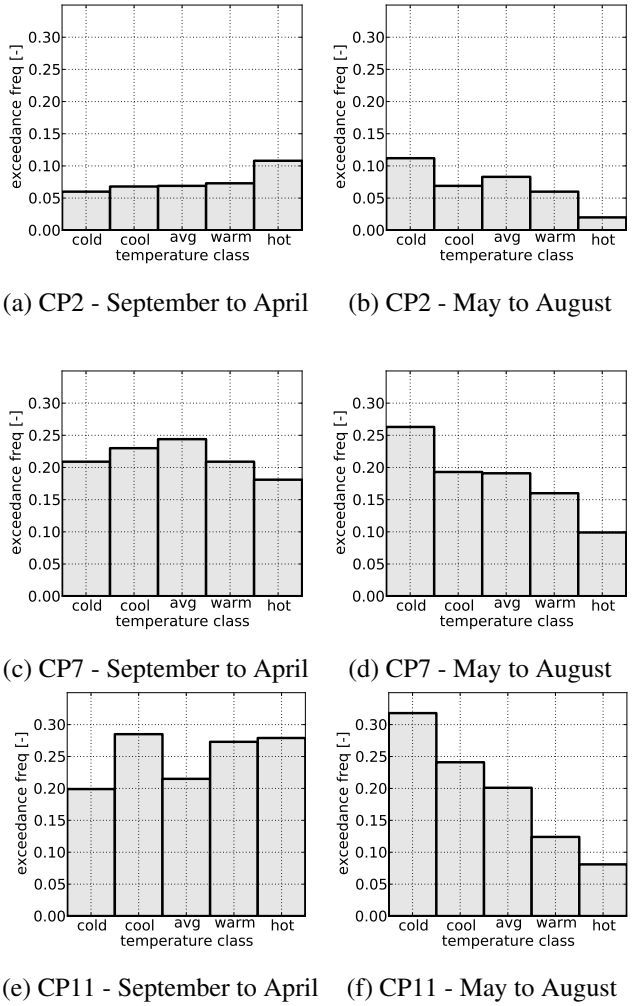

(a) CP2 - September to April (b) CP2 - May to August

(c) CP7 - September to April (d) CP7 - May to August

(e) CP11 - September to April (f) CP11 - May to August

Fig. 6. Frequency of $R \geq 0.1$ mm according to three different CPs and two seasons.

"alpha" below the equation of the regression function is the significance of rejecting the hypothesis that the slope of the true regression line is zero.

Figure 5 suggests that the atmospheric circulation has shifted between 1958 and 2004. The number of days with anticyclonic CPs has increased, during the summer months by almost two days in every five years. The number of days with cyclonic CPs has decreased. Taking $\alpha = 5\,\%$ as a limit, there is a significant increasing trend in high-pressure situations in both seasons and a decreasing trend in low-pressure situations from May to August.

3.3 Reaction of temperature

The effect of the temperature subdivision on the empirical distribution of each CP is demonstrated by the example of CP2, CP7 and CP11. It is tested by the hourly precipitation frequency with a threshold of 0.1 mm (Fig. 6) and the exceedance frequency of the 95 % and 99 % quantile referring to all wet hours ($R \geq 0.1$ mm) (Fig. 7 and Fig. 8).

All three tested CPs react to temperature, with a particularly strong signal during summer months. From May to August there is a pronounced drop in precipitation frequency with increasing temperature (right column of Fig. 6). The exceedance frequency of the 95 % quantile is more than two times higher during *hot* days than during *cold* days in any of the CPs (right column of Fig. 7). It seems that the highest hourly sums are affected the most. The differences between *cold* and *hot* days in the 99 % (right column of Fig. 8) quantile are far more pronounced than in the 95 % quantile, going up to an increase by a factor of 12 for CP11. From May to August the elevated exceedance frequency of the 99 % quantile during days of CP7 and CP11 overcompensates the decrease in overall precipitation frequency. Referring to all hours, the highest hourly sums occur more often – even if it rains more rarely than average on *hot* days.

During summer all three CPs react in the same way, although not to the same extent. Higher temperatures lead to fewer rainy hours, but shift the distribution towards higher precipitation amounts. Between September and April, the reaction to temperature is less pronounced and more varying among the CPs. For CP2 the rainfall frequency slightly increases, while for CP7 and CP11 it is more or less constant (left column of Fig. 6). During days of CP2 and CP7 high precipitation values are more frequent for higher temperature (left column of Fig. 7 and Fig. 8). During CP11 the exceedance frequency of the 95 % quantile is constant (Fig. 7e). The exceedance frequency of the 99 % quantile is higher the more the temperature deviates from the average (Fig. 8e).

The seasonal differences indicate that the reaction to atmospheric temperature depends on the precipitation genesis. Due to the higher solar radiation, convective events are predominant between May and August, and that is when the temperature classification has the strongest effect on the frequency of high hourly precipitation amounts. The findings are in agreement with physical considerations. Trenberth (1999) states that an increase in atmospheric temperature should lead to fewer but more intensive rainfall events due to the stronger convective uplift and the higher moisture capacity of a warmer atmosphere. Thus, although the classification is merely based on statistical properties, it leads to physically sound results.

Nevertheless, the CP and temperature classification is not able to completely separate the effects of higher atmospheric temperature and changes in the atmospheric circulation. The atmospheric temperature over central Europe is not only a measure of the moisture capacity and the potential strength of convective uplift, but also an indicator of the origin of the arriving air masses. Since the days belonging to one CP class do not have completely identical pressure maps, the flow field of each CP can vary to a certain extent. Lower temperatures in winter for example may indicate a shift of the flow direction to the north, which alters the path of the arriving air

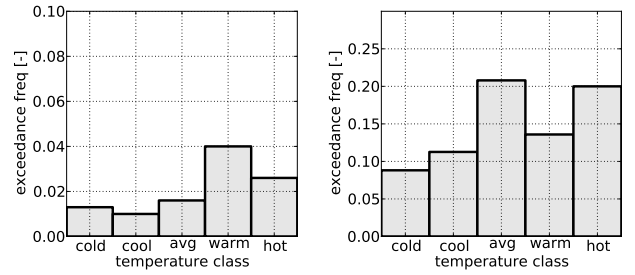

(a) CP2 - September to April (b) CP2 - May to August

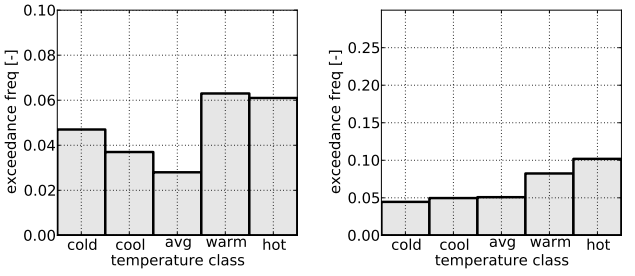

(c) CP7 - September to April (d) CP7 - May to August

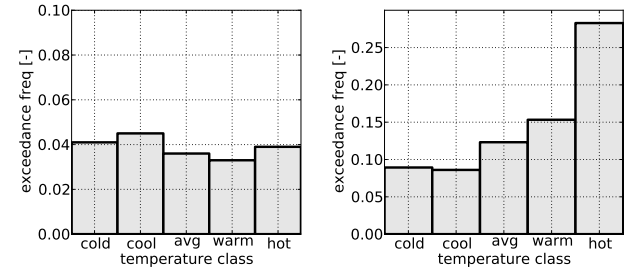

(e) CP11 - September to April (f) CP11 - May to August

Fig. 7. Exceedance frequency of the 95 % quantile according to three different CPs and two seasons; the exceedance frequency refers to all hours with $R \geq 0.1$ mm.

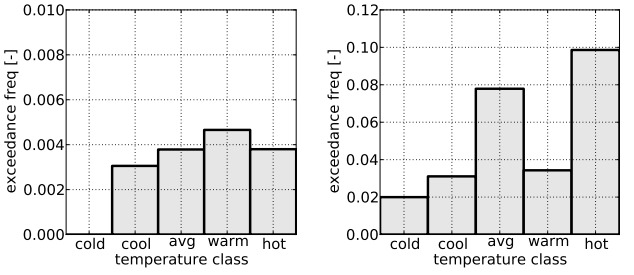

(a) CP2 - September to April (b) CP2 - May to August

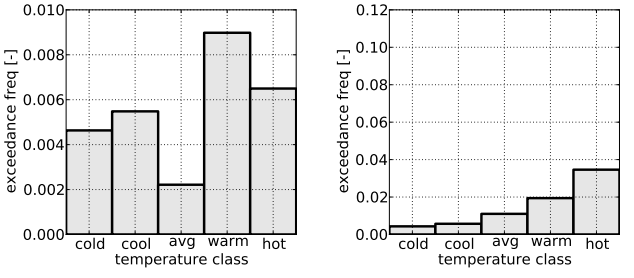

(c) CP7 - September to April (d) CP7 - May to August

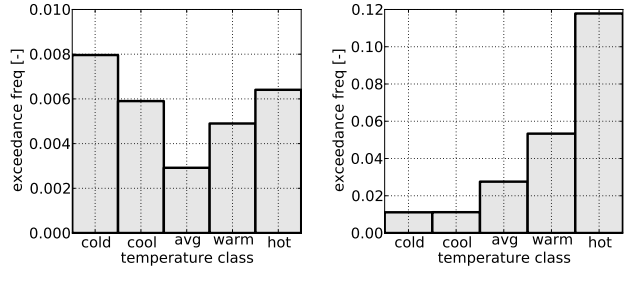

(e) CP11 - September to April (f) CP11 - May to August

Fig. 8. Exceedance frequency of the 99 % quantile according to three different CPs and two seasons; the exceedance frequency refers to all hours with $R \geq 0.1$ mm.

masses over the sea and, therefore, the evaporation and the moisture content. This might explain some of the variability in the CPs' reaction to temperature, especially in winter months when the energy input by radiation as the driving force for convection is low.

Furthermore, daily temperatures do not capture all temperature-dependent effects. The particularly high 99 % quantile exceedance frequency during *cold* days of CP11 (Fig. 8e) is an example. CP11 leads to northern fluxes. If the atmosphere was warm before, the drop in temperature when the northern flux sets in releases much water due to the decreasing storage capacity of the air. The amount of released atmospheric water is rather a function of the temperature difference in this case and depends on the amount of available water that is present from the days before. For a more detailed classification, it could be beneficial to consider the temperature history before a precipitation event.

4 CP classification according to ECHAM5

4.1 Expected CP sequence

The CP-temperature classification will only give a valid prognosis for future precipitation if ECHAM5 is able to predict the CP sequence in a realistic manner. For a comparison with observations the CP-defining fuzzy rule set is applied to gridded MLSP data from the ECHAM5 20th-century run. Fig. 9 presents the resulting absolute yearly frequencies of anticyclonic (CP2, CP3, CP5 and CP8) and cyclonic CPs (CP7, CP10, CP11 and CP12) between 1961 and 2000. In comparison, the results derived from the NCEP/NCAR reanalysis (Fig. 5) are seen as a reference for the observed CP sequence. Since the 20th-century run is a free simulation (except for the CO_2 forcing), it cannot be expected that the absolute frequencies according to ECHAM5 are the same as in the reanalysis data. On average over several years, however,

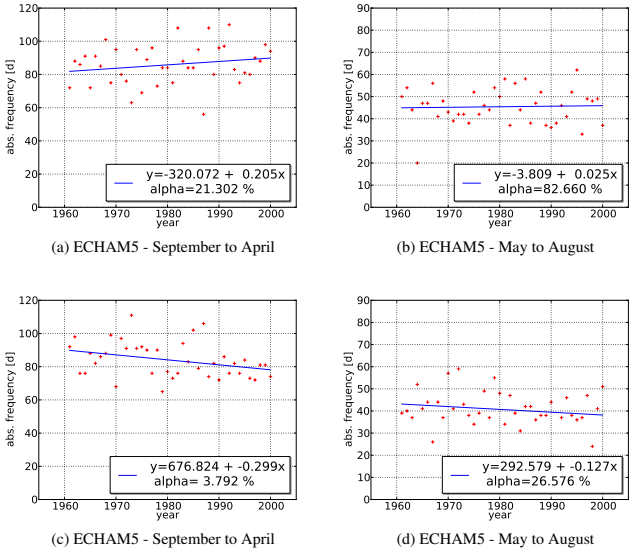

(a) ECHAM5 - September to April (b) ECHAM5 - May to August

(c) ECHAM5 - September to April (d) ECHAM5 - May to August

Fig. 9. Trends in the frequency of anticyclonic (CP2,CP3, CP5 and CP8 – first line) and cyclonic CPs (CP7, CP10, CP11 and CP12 – second line) according to the 20th-century run of ECHAM5 during two seasons.

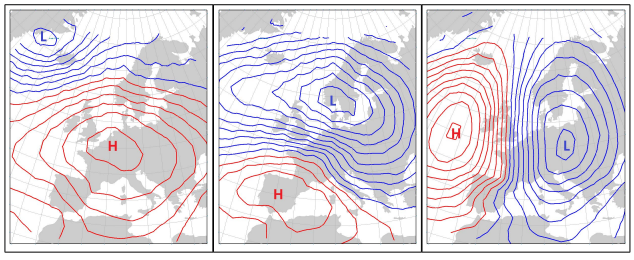

(a) CP2 (b) CP7 (c) CP11

Fig. 10. 1 hPa isobars of the mean sea level pressure anomalies of CPs related to high precipitation intensities according to the 20th-century run of ECHAM5.

the frequencies should be comparable and the trend signals similar if the GCM gives a valid representation of the atmospheric circulation.

ECHAM5 reproduces the average frequencies of cyclonic and anticyclonic CPs correctly (Fig. 9), but has limited capacity to represent the observed trend signals. Between September and April the trend is underestimated (Fig. 9a); in summer months it is completely missed (Fig. 9b). For the anticyclonic CPs ECHAM5 models a decreasing trend from September to April (Fig. 9c) that cannot be seen in the reanalysis data. The observed decreasing trend in summer, on the other hand, is underestimated (Fig. 9d).

As the CPs are defined on the basis of normalized pressure anomalies and not on absolute pressure values, the problems of ECHAM5 in reproducing the CP frequencies do not come from different mean conditions. Fig. 10 displays the average MLSP anomaly fields in the 20th-century run of ECHAM5 of

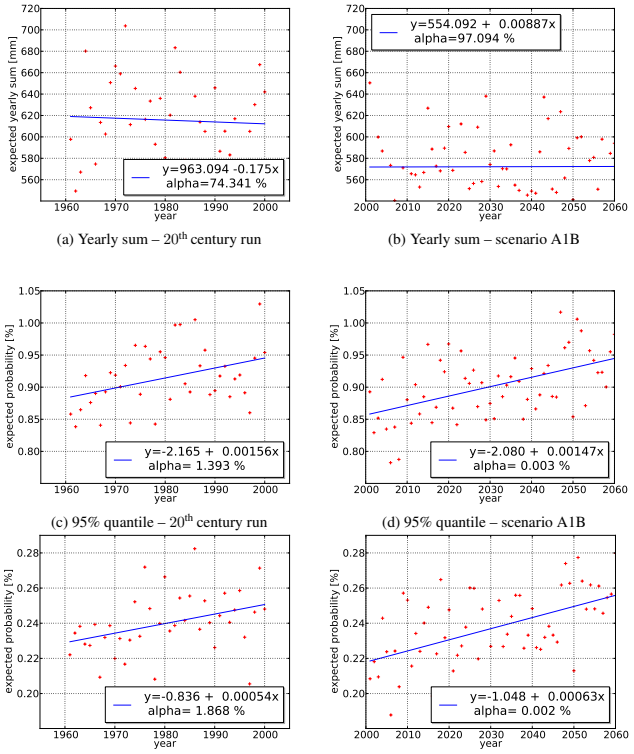

(a) Yearly sum – 20th century run (b) Yearly sum – scenario A1B

(c) 95% quantile – 20th century run (d) 95% quantile – scenario A1B

(e) 99% quantile – 20th century run (f) 99% quantile – scenario A1B

Fig. 11. Linear trend in the expected yearly precipitation sum and the yearly probability of values exceeding the 95 % and 99 % quantile according to the CP-temperature sequence derived from ECHAM5; quantiles refer to the calibration period from 1991 to 2003.

all days that are classified as CP2, CP7 and CP11. The maps look very similar to the pressure maps from the reanalysis (Fig. 3). The centers of the high- and low-pressure zones are at the same locations and the shapes are comparable. Thus, ECHAM5 produces the average MSLP fields very well, but not the temporal sequence of the MSLP fields.

4.2 Expected trend in 1 h rainfall depths

The fuzzy rule set and the temperature classification are applied on two ECHAM5 data sets, the 20th-century run from 1961 to 2000 and the scenario A1B run from 2001 to 2060, to extract a 100 yr-long time series of CP-temperature classes. The temperature subdivision is based on the surface temperature anomalies of the ECHAM5 runs in reference to the average annual cycle during of the 20th-century run. The CP-specific temperature class limits are estimated as the quantiles during the 20th-century run and then kept constant during the scenario run. This means that the distribution will shift if temperature rises. *Cold* and *cool* days will become less frequent, and *warm* and *hot* days more frequent.

According to the downscaling method described in Sect. 2.5 the CP-temperature sequence is transferred into a

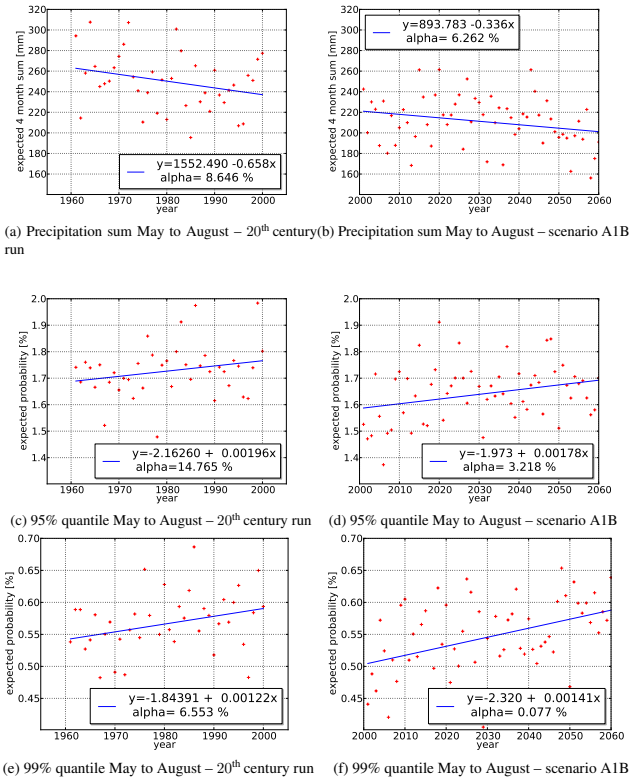

(a) Precipitation sum May to August – 20th century run (b) Precipitation sum May to August – scenario A1B run

(c) 95% quantile May to August – 20th century run (d) 95% quantile May to August – scenario A1B

(e) 99% quantile May to August – 20th century run (f) 99% quantile May to August – scenario A1B

Fig. 12. Linear trend during summer months in the expected precipitation sum and the yearly probability of values exceeding the 95 % and 99 % quantile according to the CP-temperature sequence derived from ECHAM5; quantiles refer to the calibration period from 1991 to 2003.

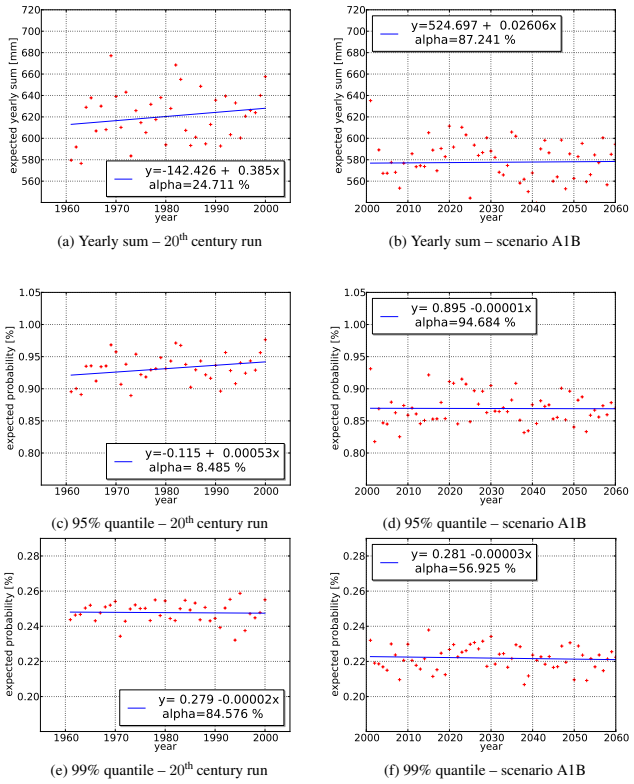

(a) Yearly sum – 20th century run (b) Yearly sum – scenario A1B

(c) 95% quantile – 20th century run (d) 95% quantile – scenario A1B

(e) 99% quantile – 20th century run (f) 99% quantile – scenario A1B

Fig. 13. Linear trend in the expected yearly precipitation sum and the yearly probability of values exceeding the 95 % and 99 % quantile according to the CP sequence derived from ECHAM5 without temperature information; quantiles refer to the calibration period from 1991 to 2003.

series of expected distributions for the years from 1961 to 2060. Fig. 11 illustrates how the combination of changing CP sequence and temperature affects the statistical expectations. The first line shows the expected yearly sum, and the second and third line the expected exceedance frequencies of the station-specific histogram class limits that mark the 95 % and 99 % quantile during the calibration period from 1991 and 2003. Since the calculation of the 95 % (99 %) quantile for the calibration period is based on wet hours only ($R \geq 0.1$ mm), the expected exceedance probabilities in respect to *all hours* in the year is lower than 5 % (1 %). An additional analysis is performed considering only the summer months from May to August (Fig. 12). Potential trends are estimated by linear regression, marked by a line in the respective diagram. "Alpha" is the significance in a two-sided hypothesis test of rejecting the hypothesis that the slope of the true regression line is zero.

The CP-temperature sequence derived from ECHAM5 consists of drier CP-temperature classes than the observed sequence. The expected yearly sums spread around 600 mm per year during the 20th century and the scenario run (Fig. 11a and b). The observed average over the 30 precipitation stations used for calibration is about 150 mm higher. The expected yearly sums vary within a realistic range of 160 mm during the 20th century and the scenario run and exhibit no significant trend. The exceedance probabilities of the 95 % and 99 % quantile of the calibration period, on the other hand, increase with time. The trend signal is strongest in the exceedance probability of the 99 % quantile during the scenario run, which increases by almost 20 % between 2000 and 2060 and with a very strong significance of $\alpha < 1$ %.

The trend signals in the exceedance probabilities of the 20th-century run and the scenario run correspond well. The slopes of the linear regression function in both periods do not differ by more than some percent. The absolute values, however, are discontinuous. At the break point between the 20th century and the A1B scenario run, from 2000 to 2001, the probabilities drop back to the level of 1960 to start increasing anew. Since the empirical histograms used for the calculation are constant, it indicates a discontinuity in the CP-temperature sequence.

The summer months between May and August are predicted to become dryer (Fig. 12a and b), which indicates a shift of the precipitation activity towards winter. Nevertheless, the exceedance probabilities of the 95 % and 99 % quantiles from the calibration period are still increasing

during summer. The increase is strongest in the 99 % quantile (Fig. 12e and f), which is a result of a shift in the distribution towards the highest hourly precipitation amounts. Although it will rain less according to ECHAM5, it will rain more heavily. Again, the regression lines between the 20th-century run and the A1B scenario run are discontinuous.

To judge whether the expected trends and the observed break point are caused rather by changes in the CP sequence or the predicted temperature rise, the analysis is repeated based on the CP classification only, ignoring the temperature subdivision (Fig. 13). The yearly sums exhibit only minor changes. Without temperature information, the 20th-century run shows a slight trend towards higher yearly sums (Fig. 13a), which has been balanced in Fig. 11a by the temperature effect. The A1B scenario predicts about the same yearly sums as with temperature information. The expected distributions of hourly rainfall depths are altered by the missing temperature information. The trends in the exceedance frequencies of the 95 % and the 99 % quantile disappear except for the 95 % quantile in the 20th-century run. This means that the trend towards higher hourly rainfall depths is mainly a reaction to the temperature signal. The break point between the 20th century and the A1B scenario run persists; thus, it is not caused by the GCM's temperature data, but most probably by differences in the representation of the atmospheric circulation between the 20th-century run and the A1B scenario run, perhaps due to different parameterization of the GCM.

5 Conclusions

An objective, automated CP classification was set up that divides all days according to their distribution of the hourly precipitation sums. The classification is based on SLP fields from reanalysis data, in this study from the NCEP/NCAR reanalysis. As an alternative, the NCAR Sea Level Pressure data (Trenberth and Paolino, 1980; https://climatedataguide.ucar.edu/climate-data/ncar-sea-level-pressure) with $5^\circ \times 5^\circ$ spatial resolution was tested, too. It led to very similar results, not only concerning the pressure maps of each CP, but also the precipitation response. In our experience, any gridded SLP data are suitable for the classification as long as the resolution is fine enough to represent the cyclonic and anticyclonic systems which are the main features of the CPs.

The CPs were further subdivided according to the atmospheric temperature. The results of the CP-temperature classification correspond well to physical considerations. During summer months, when convection plays a major role in precipitation genesis, there is a strong reaction to atmospheric temperature. On *hot* days it rains less frequently, but the frequency of extreme intensities is nevertheless higher. The reaction also depends on the CP. Anticyclonic CPs exhibit strong enhancement of extremes. CPs with western fluxes, leading to frontal rainfall, show the lowest enhancement. Outside the main convective season, from September to April, the reaction to temperature is less pronounced and more varying between the CPs. An increase in precipitation with higher temperature, which would be indicated by the Clausius–Clapeyron relation, could not be observed for all CPs. Probably, the CP-temperature classification is not able to completely separate the effect of circulation and temperature. Slight changes in atmospheric circulation also affect the temperature, but do not necessarily change the CP class.

The CP-temperature classification was used as a spatial-temporal downscaling scheme for a prognosis of hourly rainfall depths in the future derived from large-scale atmospheric circulation and temperature. The method was applied on the data from two runs of ECHAM5, the 20th-century run and the scenario A1B run. In this study, the developed downscaling method is applied to a set of 30 rainfall stations in south-western Germany that represent the average conditions of an area of about 35 000 km^2. With the same methodology it is also possible to provide precipitation data on the local scale if the empirical histograms are calculated for one single rainfall station. However, the restriction to one single location introduces a higher sampling uncertainty as the empirical precipitation frequencies of each CP-temperature combination are much lower. Since a stable estimation of the empirical histograms to each CP-temperature combination is crucial for the performance, the time series used for calibration have to be much longer and the number of CPs should be reduced, e.g. by regrouping the CP-temperature classes according to similarities in the empirical distributions.

According to ECHAM5, there will be a change in the annual cycle during the next decades. The winter months will become wetter; the summer months will become dryer. At the same time, a shift in the distribution is predicted towards the highest hourly rainfall depths, especially during summer. The findings are in agreement with previous investigations. The shift of precipitation from summer to winter is consistent with observed trends (Hundecha and Bárdossy, 2005) and confirmed by a direct analysis of RCM precipitation (Déqué et al., 2007). The predicted increase in extreme precipitation, and the related shift in scaling towards more intensive short-term events, follows a trend that has been observed in past data (Beck, 2013) and is consistent with physical considerations (Trenberth, 1999).

If the predictions are right, it will have severe consequences for all domains in which short-term precipitation intensities play a major role. Besides urban hydrology with small catchments and fast response times, agricultural production will be severely affected. The lower precipitation volume during summer months in combination with increased evaporation due to higher temperatures will augment the risk of water stress. Simultaneously, the probability for extreme precipitation intensities increases, which means that crops will be damaged more frequently during rain storm events. For farmers this is problematic. They face a higher

effort for irrigation in combination with more frequent losses of income due to bad harvests.

Nevertheless, such an indirect downscaling by CP and temperature implies two major assumptions: firstly, that ECHAM5 is able to predict the CP sequence and the surface temperature of the future in a realistic manner and, secondly, that the precipitation distribution of each CP-temperature class is constant over time, which means that changes in the CP sequence and atmospheric temperature fully explain the changes in precipitation.

With regard to the first assumption, the capacity of ECHAM5 to represent the "true" CP sequence is limited. The CP frequencies are realistically modeled compared to the CP sequence based on NCEP/NCAR reanalysis data. Observed trends, however, e.g. an increase in high-pressure situations during summer months, are missed. With the given data it cannot be judged whether the differences between observed and simulated CP series are due to model errors. The verification period of 40 yr is too short to rule out the deviations being merely a result of the different representation of inter-decennial variability between NCEP/NCAR and ECHAM5.

The second assumption cannot be verified either, but there is indication that it is only valid as an approximation. The temperature classes have been defined according to the quantiles in the temperature anomaly distribution of the past. Per definition they are equally distributed. With the predicted temperature rise during the scenario run, the distribution will shift. *Cold* days become less frequent in the future and represent atmospheric conditions that are farther away from the CP's average than *cold* days of the past. Since variations in the large-scale atmospheric circulation can affect the regional temperature conditions, *cold* days in the future might exhibit a different precipitation response than *cold* days of the past. Furthermore, if the temperatures in the future exceeds the observed temperature range, it might lead to new situations that have not yet occurred in the past, which would change the statistical response of all CPs during *hot* days.

A clear problem of ECHAM5 is the inconsistency between the 20th century and the A1B scenario run. In most of the statistics, there is a pronounced jump between the two ECHAM5 runs. Probably, the results of the years 1961 to 2000 do not exhibit the same bias or model errors as the results of the years 2001 to 2060, which makes the interpretation difficult. If both data sets are regarded as one 100 yr-long time series, no significant trend signals are found. The increase during the single runs is canceled by the jump at the break point between 2000 and 2001. Most probably, the discontinuity reflects differences in the representation of MSLP in the 20th century and the A1B scenario run, potentially caused by differences in the GCM's parameterization or by the internal stochastic variability of ECHAM5. Concerning precipitation, stochastic variations between several runs of the same model can attain a range similar to the difference between climate models (Deser et al., 2012). MSLP data are regarded as more reliable (Kendon and Clark, 2008); however, if it is affected by internal variability, the jump in the predicted statistics between 2000 and 2001 could arise from purely random effects.

In any case, the assumption that the model bias is constant over time is a necessary condition for most statistical downscaling techniques. If this assumption is disproved by GCM data, the results of many statistical methods become doubtful, e.g. the delta change or the analogous method.

In perspective of the potential model errors and stochastic variability, this study can only be a first step. It proved that the proposed downscaling scheme is able to create physically sound results. These results, however, have to be verified by subsequent investigations including other scenarios than A1B and data from different GCM. The long-term objective of this research is to implement such a downscaling scheme in the data-driven time series generator NiedSim (Bárdossy, 1998) to provide synthetic precipitation data that reflect predictions of future climatic conditions.

Acknowledgements. This work was kindly supported by the Landesanstalt für Umwelt, Messungen und Naturschutz Baden-Württemberg (LUBW) as well as by the German Research Foundation (DFG) within the funding program Open Access Publishing.

Edited by: N. Verhoest

References

Aarts, E. and van Laarhoven, P.: Simulated annealing: An introduction, Statistica Neerlandica, 43, 31–52, 1989.

Bárdossy, A.: Generating Precipitation Time Series Using Simulated Annealing, Water Resour. Res., 34, 1737–1744, 1998.

Bárdossy, A.: Atmospheric circulation patterns classification for South-West Germany using hydrolodical variables, Phys. Chem. Earth, 35, 498–506, 2010.

Bárdossy, A. and Filiz, F.: Identification of flood producing atmospheric circulation patterns, J. Hydrol., 313, 48–57, 2005.

Beck, F.: Generation of spatially correlated synthetic rainfall time series in high temporal resolution: a data driven approach, Ph.D. thesis, Universität Stuttgart, Holzgartenstr. 16, 70174 Stuttgart, available at: http://elib.uni-stuttgart.de/opus/volltexte/2013/8216, 2013.

Déqué, M., Rowell, D., L uthi, D., Giorgi, F., Christensen, J., Rockel, B., Jacob, D., Kjellstr om, E., de Castro, M., and van den Hurk, B.: An intercomparison of regional climate simulations for Europe: assessing uncertainties in model projections, Clim. Change, 81, 53–70, doi:10.1007/s10584-006-9228-x, 2007.

Deser, C., Phillips, A., Bourdette, V., and Teng, H.: Uncertainty in climate change projections: the role of internal variability, Clim. Dynam., 38, 527–546, 2012.

Fowler, H. J., Ekstr om, M., and Blenkinsop, S.: Estimating change in extreme European precipitation using a multimodel ensemble, J. Geophys. Res., 112, D18104, doi:10.1029/2007JD008619, 2007.

Groppelli, B., Bocchiola, D., and Rosso, R.: Spatial downscaling of precipitation from GCMs for climate change projections using random cascades: A case study in Italy, Water Resour. Res., 47, W03519, doi:10.1029/2010WR009437, 2011.

Guichard, F., Petch, J. C., Redelsperger, J.-L., Bechtold, P., Chaboureau, J.-P., Cheinet, S., Grabowski, W., Grenier, H., Jones, C. G., K ohler, M., Piriou, J.-M., Tailleux, R., and Tomasini, M.: Modelling the diurnal cycle of deep precipitating convection over land with cloud-resolving models and single-column models, Q. J. Roy. Meteorol. Soc., 130, 3139–3172, 2004.

Held, I. M. and Soden, B. J.: Robust Responses of the Hydrological Cycle to Global Warming, J. Climate, 19, 5686–5699, 2006.

Hundecha, Y. and Bárdossy, A.: Trends in daily precipitation and temperature extremes across western Germany in the second half of the 20th century, Int. J. Climatol., 25, 1189–1202, 2005.

Kendon, E. and Clark, R.: Reliability of future changes in heavy rainfall over the UK, in: BHS 10th National Hydrology Symposium, Exeter, 2008.

Kendon, E., Rowell, D., and Jones, R.: Mechanisms and reliability of future projected changes in daily precipitation, Clim. Dynam., 35, 489–509, doi:10.1007/s00382-009-0639-z, 2010.

Kistler, R., Kalnay, E., Collins, W., Saha, S., White, G., Woollen, J., Chelliah, M., Ebisuzaki, W., Kanamitsu, M., Kousky, V., van den Dool, H., Jenne, R., and Fiorino, M.: The NCEP–NCAR 50-Year Reanalysis: Monthly Means CD-ROM and Documentation, B. Am. Meteorol. Soc., 82, 247–268, 2001.

Lenderink, G. and van Meijgaard, E.: Increase in hourly precipitation extremes beyond expectations from temperature changes, Nat. Geosci., 1, 511–514, 2008.

Lenderink, G., Buishand, A., and van Deursen, W.: Estimates of future discharges of the river Rhine using two scenario methodologies: direct versus delta approach, Hydrol. Earth Syst. Sci., 11, 1145–1159, doi:10.5194/hess-11-1145-2007, 2007.

Lenderink, G., Mok, H. Y., Lee, T. C., and van Oldenborgh, G. J.: Scaling and trends of hourly precipitation extremes in two different climate zones – Hong Kong and the Netherlands, Hydrol. Earth Syst. Sci., 15, 3033–3041, doi:10.5194/hess-15-3033-2011, 2011.

Molnar, P. and Burlando, P.: Preservation of rainfall properties in sthochastic disaggregation by a simple random cascade model, Atmos. Res., 77, 137–151, 2005.

Nguyen, V.-T.-V., Nguyen, T.-D., and Cung, A.: A statistical approach to downscaling of sub-daily extreme rainfall processes for climate-related impact studies in urban areas, Water Sci. Technol.: Water Supply, 7, 183–192, 2007.

Roeckner, E., B auml, G., Bonaventura, L., Brokopf, R., Esch, M., Giorgetta, M., Hagemann, S., Kirchner, I., Kornblueh, L., Manzini, E., Rhodin, A., Schlese, U., Schulzweida, U., and Tompkins, A.: The atmospheric general circulation model ECHAM5, Tech. rep., Max-Planck-Institut für Meteorologie, 2003.

Trenberth, K. E.: Conceptual Framework for Changes of Extremes of the Hydrological Cycle with Climate Change, Clim. Change, 42, 327–339, doi:10.1023/A:1005488920935, 1999.

Trenberth, K. E., Dai, A., Rasmussen, R. M., and Parsons, D. B.: The Changing Character of Precipitation, B. Am. Meteorol. Soc., 84, 1205–1217, 2003.

Trendberth, K. and Paolino, D. A.: The Northern Hemisphere Sea-Level Pressure Data Set: Trends, Errors and Discontinuities, Mon. Weather Rev., 108, 855–872, 1980.

Wentz, F. J., Ricciardulli, L., Hilburn, K., and Mears, C.: How Much More Rain Will Global Warming Bring?, Science, 317, 233–235, 2007.

Willems, P. and Vrac, M.: Statistical precipitation downscaling for small-scale hydrological impact investigations of climate change, J. Hydrol., 402, 193–205, 2011.